CHEMISTRY OF MATERIALS
Article

Chem. Mater. **2009,** *21,* 2733–2745 2733
DOI:10.1021/cm900279u

Electrochemical and Structural Study of the Layered, "Li-Excess" Lithium-Ion Battery Electrode Material $Li[Li_{1/9}Ni_{1/3}Mn_{5/9}]O_2$

Meng Jiang,[†] Baris Key,[†] Ying S. Meng,[‡] and Clare P. Grey*[,†]

[†]*Department of Chemistry, SUNY Stony Brook, Stony Brook, New York 11794-3400, and* [‡]*Department of Materials Science and Engineering, University of Florida, Gainesville, Florida 32611*

Received January 29, 2009. Revised Manuscript Received May 7, 2009

The overcapacity mechanism and high voltage process of the Li-excess electrode material $Li[Li_{1/9}Ni_{1/3}Mn_{5/9}]O_2$ are studied by solid-state NMR, X-ray diffraction, X-ray absorption spectroscopy, transmission electron microscopy, combined with galvanostatic and potentiostatic intermittent titration electrochemical measurements. The cycling performance is improved noticeably when the material is cycled between potential windows of 5.3−2.5 V compared to 4.6−2.5 V. Diffraction data show that structural changes occur at high voltages, the solid-state NMR data of the same samples indicating that the high voltage processes above 4.4 V are associated with Li removal from the structure, in addition to electrolyte decomposition. The NMR spectra of the discharged samples show that cation rearrangements in the transition metal layers have occurred. The XAS spectra confirm that the Mn oxidation state remains unchanged at 4+, whereas Ni^{2+} is oxidized to Ni^{4+} on charging to 4.4 V, returning to Ni^{2+} on discharge, independent of the final charge voltage. A significant change of the shape of the Ni edge is observed in the 4.6−5.3 V potential range on charge, which is ascribed to a change in the Ni local environment. No O_2 evolution was detected based on ex situ analysis of the gases evolved in the batteries, the TEM data showing that thick passivating films form on the electrodes. The results suggest that at least some of the oxygen loss from these lithium-excess materials occurs via a mechanism involving electrolyte decomposition.

1. Introduction

Layered lithium nickel manganese oxides have attracted interest as possible alternatives to $LiCoO_2$, the material that is most commonly used as a positive electrode in commercial Li ion batteries, because of their lower cost and higher safety and abuse tolerance, when lithium is removed from their structure.[1] The series of compounds $Li[Li_{1/3-2x/3}Ni_xMn_{2/3-x/3}]O_2$ were first reported by Lu and Dahn, and Ohzuku et al. in 2001.[2,3] These layered structures are derived from $LiCoO_2$ (space group $R\bar{3}m$); however, the additional Li ions present in the transition metal (TM) layers induce cation ordering in the TM layers. This results in additional superstructure peaks in their diffraction patterns characteristic of the honeycomb Li/Mn ordering found in the end member compound Li_2MnO_3 (or $Li[Li_{1/3}Mn_{2/3}]O_2$, using the layered notation). Ni^{2+}/Ni^{4+} is generally considered to be the active redox couple that compensates for the deintercalation/intercalation of Li ions from/into the structure.[4] However, in the phases with $x < 1/2$, the so-called Li-excess compounds, the fraction of Li ions extracted, particularly in the first charge, is noticeably higher than the theoretical capacity calculated based on the Ni^{2+}/Ni^{4+} couple.[3,5−7] A flat, plateau-like region starting from 4.4 V is always observed in the first charge, but this process is not reversible and is not seen in the first discharge and in subsequent cycles. Given the technological interest associated with these materials, much scientific effort has been devoted to determine where this overcapacity comes from. Lu et al. proposed an oxygen loss mechanism (removal of Li_2O) to balance the charge,[3,6,7] which is supported by Armstrong et al.'s observations of oxygen gas evolution made with in situ electrochemical mass spectroscopy measurements.[8] Unfortunately, the amount of oxygen gas produced was not quantified in these latter experiments, so it was not possible to determine whether the oxygen evolution accounts for all of the extra capacity. These authors also showed by using neutron and X-ray diffraction that the phase remained layered after the oxygen-loss process. However, significant questions remain: for example, how does migration

*Corresponding author. E-mail: cgrey@notes.cc.sunysb.edu.

(1) Amine, K.; Liu, J.; Belharouak, I.; Kang, S. H.; Bloom, I.; Vissers, D.; Henriksen, G. *J. Power Sources* **2005**, *146*, 111–115.
(2) Ohzuku, T.; Makimura, Y. *Chem. Lett.* **2001**, *8*, 744–745.
(3) Lu, Z. H.; MacNeil, D. D.; Dahn, J. R. *Electrochem. Solid-State Lett.* **2001**, *4*(12), A200–A203.
(4) Yoon, W. S.; Paik, Y.; Yang, X. Q.; Balasubramanian, M.; McBreen, J.; Grey, C. P. *Electrochem. Solid-State Lett.* **2002**, *5*, (11), A263–A266.
(5) Lu, Z. H.; Beaulieu, L. Y.; Donaberger, R. A.; Thomas, C. L.; Dahn, J. R. *J. Electrochem. Soc.* **2002**, *149*(6), A778–A791.
(6) Lu, Z. H.; Dahn, J. R. *J. Electrochem. Soc.* **2002**, *149*(7), A815–A822.
(7) Robertson, A. D.; Bruce, P. G. *Electrochem. Solid-State Lett.* **2004**, *7*(9), A294–A298.
(8) Armstrong, A. R.; Holzapfel, M.; Novak, P.; Johnson, C. S.; Kang, S. H.; Thackeray, M. M.; Bruce, P. G. *J. Am. Chem. Soc.* **2006**, *128*(26), 8694–8698.

© 2009 American Chemical Society
Published on Web 06/09/2009

of oxygen, nickel, and manganese ions occur to form the new layered phase? If an ideal layered structure is formed at the top of the charge, why does it accommodate only approximately 0.6−0.7 Li on subsequent deintercalation?

$Li[Li_{1/9}Ni_{1/3}Mn_{5/9}]O_2$ was chosen as a representative model compound in this work, in order to investigate the structural changes that occur during the first charge−discharge cycle in series of compounds. ^{6}Li Magic Angle Spinning (MAS) Nuclear Magnetic Resonance (NMR), high resolution X-ray diffraction (XRD), X-ray absorption spectroscopy (XAS), and high resolution TEM experiments were all performed to study the short- and long-range structural and the accompanying morphology changes of the crystals during and after the high voltage process.

2. Experimental Section

2.1. Sample Preparation. *$Li[Ni_{1/3}Li_{1/9}Mn_{5/9}]O_2$.* $LiOH\cdot H_2O$ (Aldrich >98.0%), $Ni(NO_3)_2\cdot 6H_2O$ (Aldrich, >98%) and $Mn(NO_3)_2\cdot 6H_2O$ (Fluka >97.%) were used as starting materials, as previously reported.[5] The transition metal nitrates were dissolved into 50 mL of distilled water and were slowly dripped (1−2 h) into a 400 mL stirred solution of aq. LiOH (about 0.2−0.4 M). A precipitate of $M(OH)_2$ with a homogeneous cation distribution was thus formed. The precipitate was removed by filtration and washed twice to get rid of the residual Li salts (LiOH and $LiNO_3$), and then was dried in air at 180 °C overnight. Stoichiometric amounts of the precipitate and $LiOH\cdot H_2O$ were mixed by grinding in a mortar. Pellets of the mixture were heated at 480 °C for 12 h. Afterward, the pellets were ground and made into new pellets. The new pellets were heated in air at 900 °C for another 12 h and quenched in liquid nitrogen. ^{6}Li enriched materials were prepared for the NMR experiments using ^{6}Li enriched $Li_2CO_3\cdot H_2O$ as the starting material.

2.2. Electrochemistry. 2032 type Lithium coin cells were used to study the electrochemical behavior of the compound and prepare cycled samples for solid-state NMR, XRD, and TEM. $Li[Li_{1/9}Ni_{1/3}Mn_{5/9}]O_2$ was mixed with either carbon (acetylene) black (Timcal, super P−Li) or graphite (10 wt %) and poly (vinylidenefluoride) binder (PVDF) (10 wt %). The graphite was used in the cell that was cycled between 4.6 and 2.5 V for 5 cycles; acetylene black was used in all the other cells. The mixture was then dispersed in acetone or NMP, dripped on a disk of aluminum foil of 9/16 in. diameter, and dried at 80 °C. The total electrode mixture on the aluminum disk is typically about 30 mg. Lithium metal ribbon (Aldrich, 99.9%) and 1 M $LiPF_6$ in a 1:1 ethyl carbonate: dimethyl carbonate (EC: DMC) solution (Ferro) were used as an anode material and electrolyte, respectively. Two pieces of Celgard separator (Celgard Inc. USA) were used as the separator. All the cell parts were assembled in an argon−filled glovebox. The coin cells were cycled galvanostatically on an Arbin battery cycler (College Station, Texas) between 2.5 and 4.6 V, or 2.5 and 5.3 V at a $C/50$ ($\sim$0.06 mA cm^{-2}) rate, where C is the theoretical specific capacity of $Li[Ni_{1/3}Li_{1/9}Mn_{5/9}]O_2$ defined on the basis of the Ni content. The samples for the NMR, XRD, and TEM studies were recovered from cycled batteries by disassembling them inside an argon-filled glovebox, and scraping the powder mixture from the aluminum disks. In contrast, the electrode foils were kept intact and used directly for the XAS experiments after rinsing with DMC (dimethyl carbonate).[9] To avoid contact with air, we sealed them between two layers of Kapton tape.

The galvanostatic intermittent titration (GITT) experiment was performed between 5.3 and 2.5 V by applying a current corresponding to a C/50 rate in intervals of 2 h, separated by a rest period of 5 h. A potentiostatic intermittent titration (PITT) experiment was also performed. This is a chronoamperometric method that is carried out by applying potential steps of 10 mV for 24 h. The time periods were curtailed when the measured current fell below the threshold limit of 0.1 μA, corresponding to a $C/200$ rate. The voltage window was set at 5.3−2.5 V.

2.3. MAS NMR Spectroscopy. ^{6}Li MAS NMR experiments were performed at an operating frequency of 29.47 MHz on a CMX-200 spectrometer (4.7 T). A 1.8 mm double resonance probe built by Samoson and co-workers (KBFI, Tallinn, Estonia) was used. All spectra were acquired at 38 kHz with a rotor synchronized echo pulse sequence (90°-τ-180°-τ-acq), where $\tau = 1/\nu_r$. A $\pi/2$ pulse width of 3.5 μs was used with pulse delays of 0.2 s. The spectra were acquired at "room temperature" (i.e., the spectra were acquired with no control of the temperature), which corresponds to a sample temperature of between 70 and 80 °C.

2.4. TEM. Electron diffraction patterns and transmission electron microscope (TEM) images were collected from both the as-prepared powders and the powders discharged to 2.5 V after being charged to 5.3 V. To minimize the exposure to air for the electrochemically charged/discharged samples, we prepared the samples in an Ar environment. The powders were suspended on a copper grid with lacey carbon and investigated by using a JEOL 2010F microscope with an accelerating voltage of 200 kV and a field emission gun.

2.5. Synchrotron XRD. High-resolution synchrotron X-ray powder diffraction (XRD) were collected at 11-BM[10,11] and 1-BM beamlines (λ = 0.619174 and 0.4017 Å, respectively) at the Advanced Photon Source (APS) at Argonne National Laboratory (ANL). For beamline 1-BM, the samples were packed in 1.0 mm diameter glass capillaries. For 11-BM, 1.0 mm diameter Kapton capillaries were used. Rietveld refinements were performed on the collected data with the EXPGUI-GSAS software.

2.6. Ex situ GC-MS Measurements of Gases Evolved from Batteries. Modified Swagelok-type cells were used to collect the gases evolving during electrochemical cycling of $Li[Li_{1/9}Ni_{1/3}Mn_{5/9}]O_2$. The cells were prepared with empty space above the positive and negative electrodes to accumulate the gases. The Swagelok body was modified to accommodate a gas chromatography (GC) septum in order to syringe out the evolved gases (Figure 1). Positive electrodes were prepared with the same electrode mixtures as used for all the other electrochemical studies, but the maximum amount of active electrode material possible with this design was used (up to 200 mg in some runs) to increase the potential gas evolution. Lithium metal was used as the anode. Glass microfiber disks (Fisher) soaked with 1 M $LiPF_6$ in 1:1 EC/DMC (ethyl carbonate:dimethyl carbonate) were used as separators. The components were assembled in an Ar glovebox. The design has about 9 mL of dead space, which for a pristine battery contains only Ar gas and low concentrations of electrolyte vapor. The accumulated gases after charging these batteries to different potentials were syringed out and transferred for analysis by using a Hamilton gastight GC syringe

(9) Balasubramanian, M.; Sun, X.; Yang, X. Q.; McBreen, J. *J. Power Sources* **2001**, *92*(1−2), 1–8.

(10) Lee, P. L.; Shu, D. M.; Ramanathan, M.; Preissner, C.; Wang, J.; Beno, M. A.; Von Dreele, R. B.; Ribaud, L.; Kurtz, C.; Antao, S. M.; Jiao, X.; Toby, B. H. *J. Synchrot. Radiat.* **2008**, *15*, 427–432.

(11) Lee, Y. J.; Grey, C. P. *J. Phys. Chem. B* **2002**, *106*(14), 3576–3582.

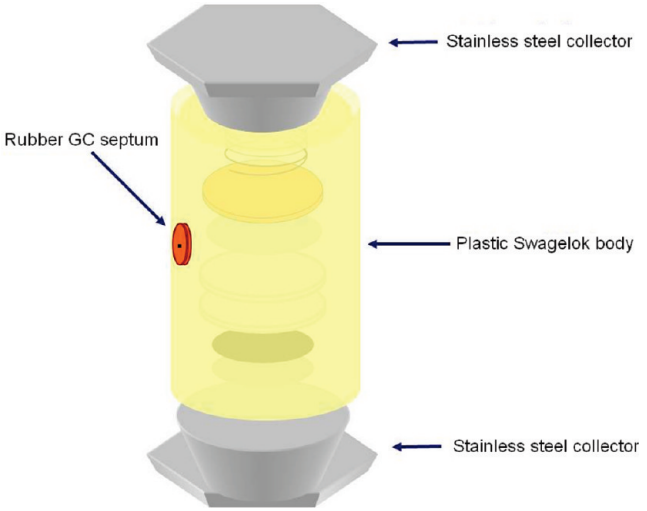

Figure 1. Swagelok cell set up for the GC-MS measurements.

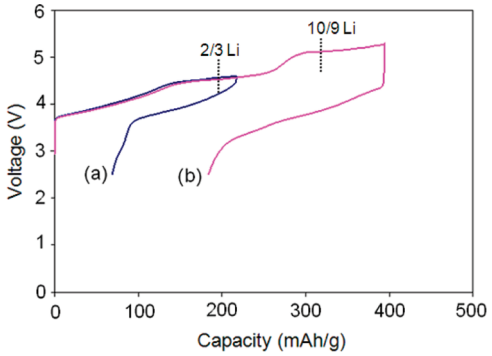

Figure 2. Electrochemical profile of $Li[Li_{1/9}Ni_{1/3}Mn_{5/9}]O_2$ with a $C/50$ rate (~0.06 mA cm^{-2}). Voltage windows of (a) 4.6−2.5 V, and (b) 5.3−2.5 V were used. The Li amounts corresponding to different "theoretical" capacities based on $Ni^{2+} \rightarrow Ni^{4+}$ oxidation (2/3 Li per formula unit) and total Li content (10/9 Li) are marked on the curves.

with miniature ball valves, and analyzed with an HP 6890 GC system with HP-GC/GASPRO fused silica capillary column, coupled with an Agilent 5973 Mass Selective Detector. The mass selective detector allowed monitoring of (without separating each gas component by chromatography) Ar, CO_2, CO, and O_2 components in the accumulated evolved gases above the electrodes.

3. Results

3.1. Electrochemistry. Figure 2 shows a comparison of the electrochemical curves resulting from applying different cut off voltages. Two types of theoretical capacities can be defined for this compound: one is based on the Ni content. Assuming that only these ions are electro-active, only 2/3 of the Li ions can be removed from the structure on oxidizing $x = 1/3$ Ni^{2+} to Ni^{4+} (per formula unit $Li[Li_{1/9}Ni_{1/3}Mn_{5/9}]O_2$), yielding a capacity of 200 mA h g^{-1}. The second definition is based on the total Li content in the material and assumes that all 10/9 Li^+ of the ions in $Li[Li_{1/9}Ni_{1/3}Mn_{5/9}]O_2$ can be removed, resulting in a capacity of 331 mA h g^{-1}. When the battery is cycled between 5.3 and 2.5 V, 400 mA h g^{-1} is obtained upon charge, and 200 mAh/g upon discharge. However, when the battery is cycled between 4.6 and 2.5 V, 230 mA h g^{-1} is obtained upon charge, but only 160 mA h g^{-1} is recovered upon discharge, which corresponds to a 20% capacity loss. The voltage increases steadily from 3.8 to 4.4 V, upon charge accounting for approximately 120 mA h g^{-1}. This is followed by a plateau-like region between 4.4 and 4.6 V. Given the voltage window of stability of the electrolyte used in these batteries, which has a maximum of around 5.0 V, it is likely that some of the capacity produced upon charge is due to its partial decomposition, accounting for the larger capacity obtained even over that assuming all the Li is removed. Nonetheless, the higher discharge capacity obtained with respect to a 4.6−2.5 V cutoff voltage indicates that part of the extra capacity obtained after 4.6 V is reversible. An additional process is observed in the electrochemical curve, from 4.9 to 5.3 V. Thus, there are at least three quite different processes during charge.

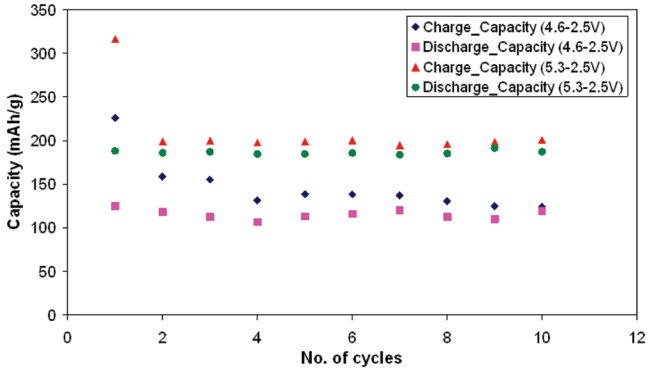

Figure 3. Comparison of the cyclability of $Li[Li_{1/9}Ni_{1/3}Mn_{5/9}]O_2$ with different voltage windows (4.6−2.5 V and 5.3−2.5 V), with a current corresponding to a $C/20$ (~0.15 mA cm^{-2}) rate.

The cyclability of $Li[Li_{1/9}Ni_{1/3}Mn_{5/9}]O_2$ in different voltage windows is compared in Figure 3. A charge and discharge capacity around 130 mAh/g could be achieved at a $C/20$ rate after 10 cycles when the window is set at 4.6−2.5 V. However, when the battery is cycled between 5.3 and 2.5 V at the same current rate, both higher charge and discharge capacities, ca. 200 mAh/g, are obtained and a better capacity retention is found after 10 cycles. To avoid further decomposition of the electrolyte at very high voltages, another battery was charged to 5.3 V only in the first cycle and then cycled between 4.8 and 2.5 V in subsequent cycles. The electrochemical profiles of different cycles are shown as an inset in Figure 4. The two plateaus seen on charge are not observed after the first cycle, and the profiles of the second and subsequent cycles are very similar, but quite distinct from that of the first cycle, indicating that the reactions that occur in the first cycle are different from those of the subsequent cycles. Additionally, the capacity obtained when cycling between 4.8 and 2.5 V is very close to that obtained in the first cycle with a 5.3−2.5 V voltage window. Thus, the reactions taking place at these high voltages can be viewed as an "activation" process that produces both an improvement in capacity and capacity retention. After the fifth cycle, the cycling rate was changed from $C/50$ to $C/13$. A decrease from 190 mA h g^{-1} at $C/50$ to 150 mA h g^{-1} at a $C/13$ rate was found.

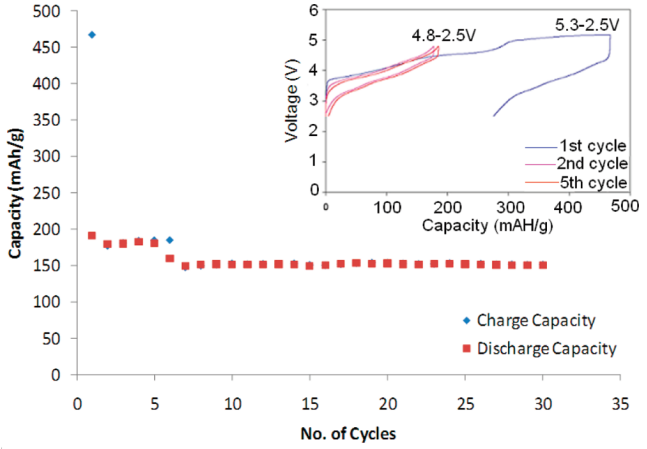

Figure 4. Cyclability of a battery charged to 5.3 V for the first charge and cycled between 4.8 and 2.5 V in the following cycles. A $C/50$ (~0.06 mA cm^{-2}) rate was used for the first four cycles and for the fifth charge process, and the subsequent rate is $C/13$ (~0.23 mA cm^{-2}). The inset shows the electrochemical profiles for the first, second, and fifth cycles.

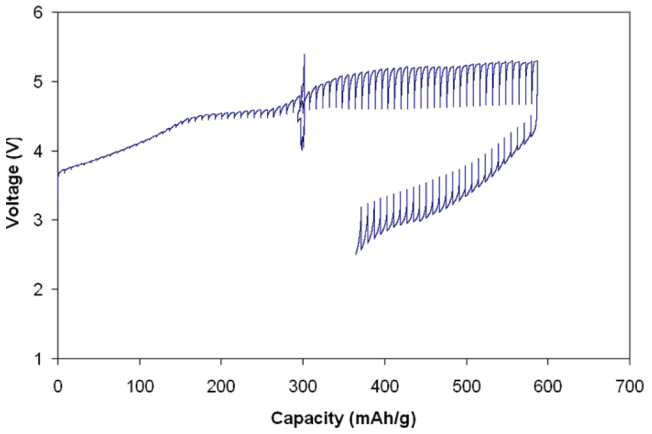

Figure 5. Galvanostatic intermittent titration (GITT) profile between 5.3 and 2.5 V, with a current corresponding to a C/50 (~0.06 mA cm^{-2}) rate. The spike at 300 mA h g^{-1} is due to a spurious current glitch of the cycler.

Both galvanostatic intermittent titration[12] (GITT) and potentiostatic intermittent titration technique[13] (PITT) experiments were performed to study the reaction mechanisms associated with the two high voltage processes observed in the electrochemical curve. Almost no overpotential is observed until 4.4 V in the GITT profile (Figure 5), the starting point of the first plateau. Above this value, an increasingly larger overpotential is found (for instance, it is about 50 mV at 4.6 V). After this point, the open circuit voltage (OCV) stabilizes at about 4.5 V and 4.6 V after 300 mA h g^{-1}, whereas the closed circuit voltage curve traces the chronopotentiometric profile shown in Figure 2. This implies that the reactions that take place at these voltages are kinetically limited. We note that the voltage termed OCV here, is actually the voltage obtained after a fixed relaxation time (5 h), and the slight increase in apparent OCV after 300 mA h g^{-1} may be due to insufficient relaxation. Figure 6a shows a zoom of the PITT profile between 3.6 and 4.0 V. The current decay at each step shows a cottrellian ($1/t^{1/2}$) dependence, which indicates that this process is a solid-solution insertion reaction.[14,15] A similar behavior was also observed in Figure 6d, which shows the curve between 3.8 and 3.5 V on discharge. These results are consistent with the gradual increase in voltage with capacity observed in the galvanostatic experiments. Panels b and c in Figure 6 show the curves between 4.4 and 4.6 V and 4.9−5.0 V where the two plateaus appear in the galvanostatic profiles. Very different behavior is now observed. The current decreases rapidly to a very low value, and then reaches the limit value slowly. This behavior is usually observed in a two-phase reaction, confirming that the high voltage processes are indeed associated with plateaus.

3.2. High-Resolution XRD. The high-resolution XRD pattern of the pristine compound is displayed in Figure 7. All the reflections can be indexed with a hexagonal rhombohedral $R\bar{3}m$ space group except for a series of additional superstructure peaks around 18−23°, 2θ, which are due to the honeycomb ordering of Li and Mn in the transition metal layers, as seen for Li_2MnO_3.[16] The ordering varies with only small changes in the heating time and the quenching method used during synthesis, leading to noticeable changes in the intensities and breadth of the superstructure reflections between sample batches.

No obvious phase transitions were observed on charging to 5.3 V, and all the patterns can still be indexed with a layered structure, even when most of the Li ions are electrochemically removed. The superstructure peaks due to the honeycomb ordering in the transition metal layers are present until 4.7 V (see inset a in Figure 8), but they almost completely disappear at 5.3 V, indicating that this ordering is lost at this voltage. This loss of the superstructure peaks at high voltage is consistent with X-ray and electron diffraction results for related "Li-excess" materials materials.[17,18]

A shoulder next to the 003 peak starts to appear at 4.4 V. This shoulder increases in intensity and shifts to lower angles from 4.4 to 5.3 V, leading to a strong asymmetry of the 003 reflection, as seen in the inset (b) of Figure 8. These peaks can not be indexed with the same cell parameters when using an $R\bar{3}m$ space group, and so they must originate from a second phase. Because only one extra peak is clearly resolved in the whole pattern, it is very difficult to identify the nature of the second phase. Separate refinements were performed, using this XRD data, assuming first that this phase arises from a layered structure with a $R\bar{3}m$ space group with slightly different cell parameters, and second, that it arises from

(12) Weppner, W.; Huggins, R. A. *J. Electrochem. Soc.* **1977**, *124*(3), C135–C135.
(13) Weppner, W.; Huggins, R. A. *J. Electrochem. Soc.* **1979**, *126*(8), C305–C305.
(14) Amarilla, J. M.; Tedjar, F.; Poinsignon, C. *Electrochim. Acta* **1994**, *39*(15), 2321–2331.
(15) Chabre, Y.; Pannetier, J. *Prog. Solid State. Chem.* **1995**, *23*(1), 1–130.
(16) Lu, Z. H.; Chen, Z. H.; Dahn, J. R. *Chem. Mater.* **2003**, *15*(16), 3214–3220.
(17) Weill, F.; Tran, N.; Martin, N.; Croguennec, L.; Delmas, C. *Electrochem. Solid-State Lett.* **2007**, *10*(8), A194–A197.
(18) Hong, Y. S.; Park, Y. J.; Ryu, K. S.; Chang, S. H. *Solid State Ionics* **2005**, *176*(11−12), 1035–1042.

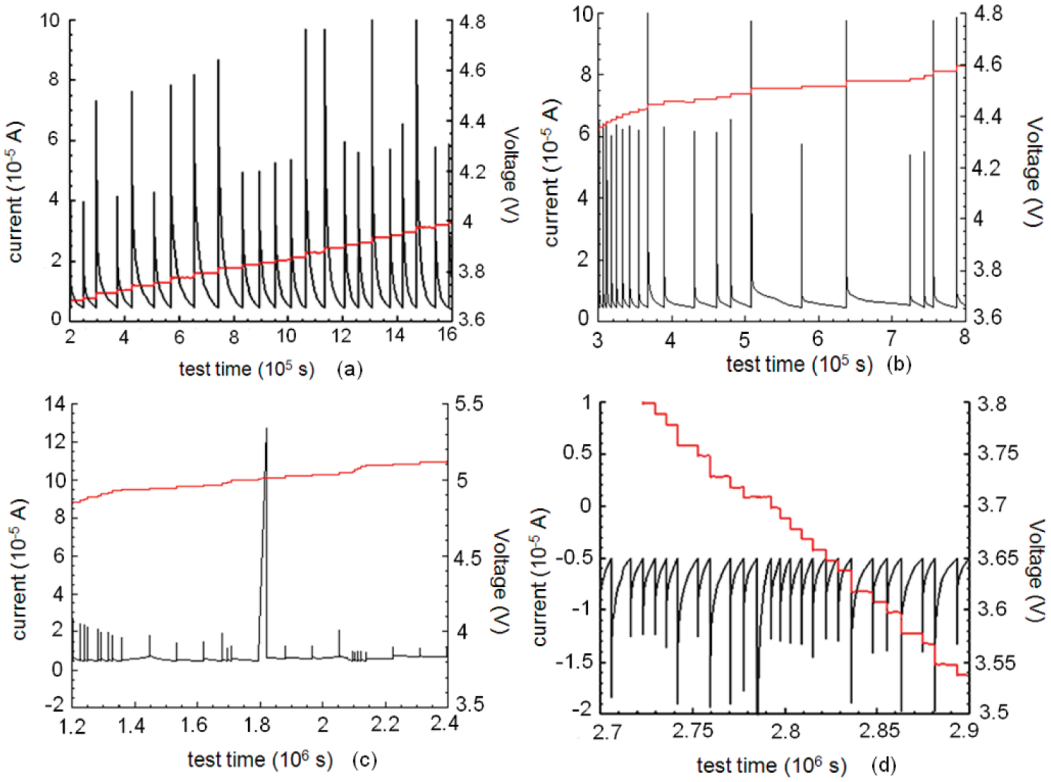

Figure 6. Potentiostatic intermittent titration technique (PITT) profiles acquired with a step size of 10 mA and current limit of 0.1 μA which corresponds to a $C/200$ (~0.015 mAcm^{-2}) rate. The four plots show the different voltage windows (a) 3.6−4.0, (b) 4.4−4.6, and (c) 4.8−5.1 V on charge and (d) 3.8−3.55 V and on discharge. In red and black are the voltage vs test time and current vs test time curves, respectively.

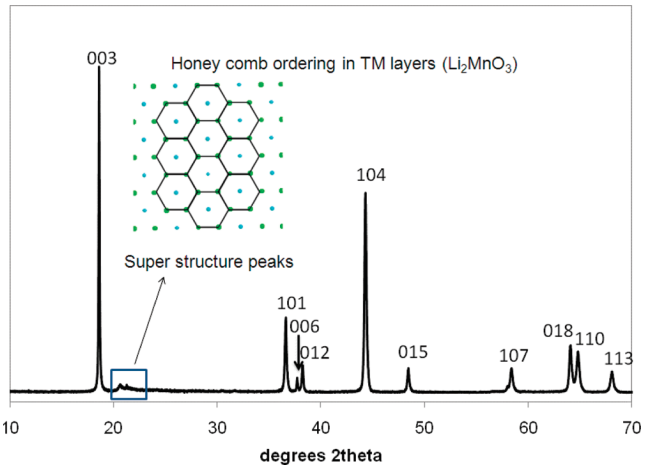

Figure 7. X-ray diffraction pattern of pristine $Li[Li_{1/9}Ni_{1/3}Mn_{5/9}]O_2$. All the peaks could be indexed with an $R\bar{3}m$ space group, except the superstructure peaks (blue box) introduced by the honeycomb ordering of the Mn and Li ions in the transition metal layers. The green and blue balls represent Mn and Li atoms respectively in the representation of the $[Li_{1/3}Mn_{2/3}]$ layer of Li_2MnO_3, shown in the inset. In this and subsequent figures, the 2θ values are converted to those corresponding to a Cu Kα wavelength (λ = 1.54 Å).

a spinel phase. Although the two refinements yielded different phase fractions for the minor component (of 20 and 5%, for the layered and spinel components, respectively), it was not possible to unambiguously determine the nature of the minor component.

The XRD patterns of the discharged samples, following charging to different potentials, are compared in Figure 9. The layered-type unit cell with an $R\bar{3}m$ space group, as in the pristine compound, could still be used to index the patterns, and only slightly different cell parameters were found. The superstructure peaks are still present in the 4.6−2.5 V sample (inset a), but they are virtually absent in the 5.3−2.5 V sample, indicating that the honeycomb ordering cannot be recovered on discharge. No shoulders are observed for the 003 peak in the discharged samples (inset b), which implies either the disappearance of the second minor phase after lithium is intercalated in the structure of this phase or that it has very similar c and a parameters.

Rietveld refinement[19] results for two discharged samples are shown in Figure 10. Both the a and c parameters increase after one cycle. A larger expansion of the unit cell is seen for the sample that has been subjected to the high voltage process, confirming the existence of a real structural change during the plateaus, quite separate from any electrolyte decomposition that may be occurring. The content of transition metal ions in both the transition metal and the Li layers were also obtained from the refinement. Because the X-ray scattering lengths of Ni and Mn are very similar, the individual contents of Ni and Mn cannot, however, be distinguished. Previous studies[20−22] have demonstrated the existence of crystallographic exchange only involving Ni and Li, leading to

(19) Rietveld, H. M. *J. Appl. Crystallogr.* **1969**, *2*, 65–&.
(20) Breger, J.; Meng, Y. S.; Hinuma, Y.; Kumar, S.; Kang, K.; Shao-Horn, Y.; Ceder, G.; Grey, C. P. *Chem. Mater.* **2006**, *18*(20), 4768–4781.
(21) Breger, J.; Kang, K.; Cabana, J.; Ceder, G.; Grey, C. P. *J. Mater. Chem.* **2007**, *17*(30), 3167–3174.
(22) Kang, K. S.; Meng, Y. S.; Breger, J.; Grey, C. P.; Ceder, G. *Science* **2006**, *311*(5763), 977–980.

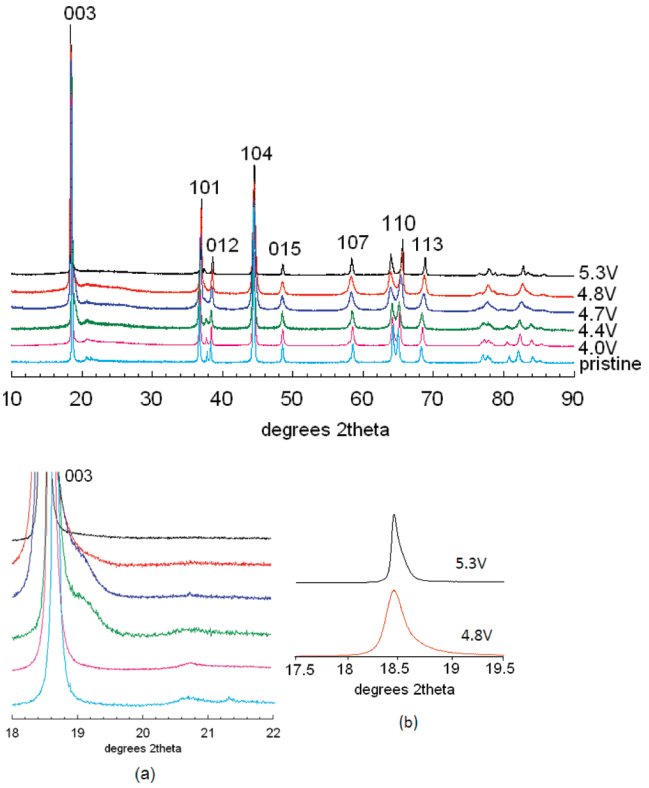

Figure 8. High-resolution XRD of charged and pristine materials. The insets show the enlargements of different 2θ regions. The XRD patterns are labeled with the cutoff voltage used to synthesize each sample.

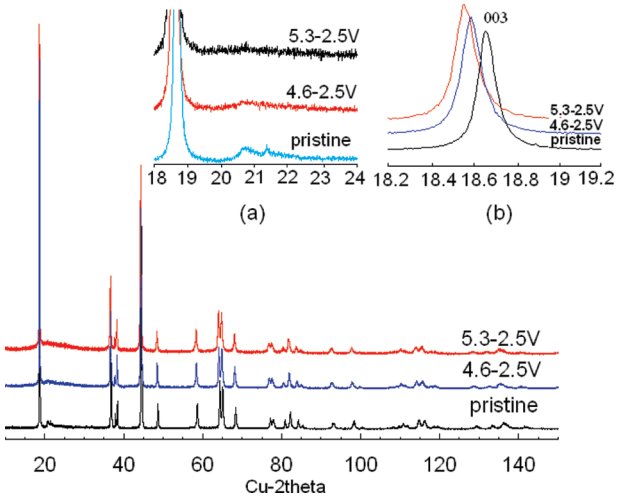

Figure 9. Comparison of the high-resolution XRD patterns of discharged samples and the pristine material. Both discharged samples were stopped at 2.5 V and the charge voltages are labeled on the patterns. The insets show enlargements of the regions containing the superstructure and 003 reflections.

the presence of the Ni in the Li layers. Hence, only this exchange was assumed in our structural models. Given the small X-ray scattering length of Li associated with its low electron density,[23] the refinements are not very sensitive to the Li content. As a consequence, the approximate Li contents used in this refinement were taken from the discharge capacity obtained in the corresponding batteries. The results of the refinements are plotted in Figure 10c. The total transition metal content in the transition metal layers of the major phase does not change after one cycle, following a charge to both 4.5 and 5.3 V, remaining constant at approximately 84−85%. In contrast, the Ni content in the Li layers increases from 5% to 9% on cycling between 2.5 and 5.3 V. Because the Ni content in these materials should remain constant, it appears that the loss of structural oxygen on charging is associated with the migration of some of the transition metal ions to the Li layers. We note that a small increase in Ni content in the Li layers was also noted in the earlier study of $Li_{1.12}(Ni_{0.425}Mn_{0.425}Co_{0.15})_{0.88}O_2$, following cycling at high voltages.[17]

The XRD patterns of the multiple cycled materials with a cutoff voltage window between 4.6 and 2.5 V are compared in Figure 11. Both cycled samples were stopped in the fully discharged state. The layered structure with $R\bar{3}m$ space group still remains after 10 cycles. However, the superstructure peaks representing honeycomb ordering in the transition metal layers are much less pronounced in the sample stopped after 5 cycles, and have totally disappeared in the 10th cycled sample. Clearly the loss of transition metal ordering can also happen after multiple cycles even when the material is cycled between the lower voltage window 4.6−2.5 V. A shoulder next to 003 peak is observed in both the 5 and 10 cycles samples, which appears at the same position as that observed in the charged samples (Figure 8), indicating that the second phase is still present in the discharged samples after multiple cycles. This suggests that this second phase is still present in the discharged samples after only one cycle (Figure 9), but that its cell parameters are similar to that of the major phase following the first cycle. However, because this phase is seen quite clearly following multiple cycles on charging to 4.6 V, this may indicate that further segregation to form larger domains of the second phase may be occurring, possibly preventing this phase from returning to the same state as observed after one cycle. Preliminary TEM studies show that spinel-like domains are formed within the particles, which may be responsible for this second phase. A more detailed TEM study of this second phase is underway and will be described in a separate paper. The role that these domains play in capacity loss or even retention after multiple cycles is currently under investigation.

3.3. ^{6}Li MAS NMR Spectroscopy. Two groups of resonances are clearly observed in the ^{6}Li NMR spectrum of $Li[Li_{1/9}Ni_{1/3}Mn_{5/9}]O_2$ (Figure 12), one at 737−587 ppm, and another at 1511−1341 ppm. On the basis of previous work,[4,11,24,25] we assign these resonances to Li ions in lithium and in the transition metal layers, respectively. The large width of the peaks at 737−587 ppm is due to the large variety of different local environments for Li ions in the Li layers, which result from the presence of varying numbers of Ni^{2+}, Mn^{4+}, and Li^+ in the first

(23) Breger, J.; Dupre, N.; Chupas, P. J.; Lee, P. L.; Proffen, T.; Parise, J. B.; Grey, C. P. *J. Am. Chem. Soc.* **2005**, *127*(20), 7529–7537.
(24) Yoon, W. S.; Kim, N.; Yang, X. Q.; McBreen, J.; Grey, C. P. *J. Power Sources* **2003**, *119*, 649–653.
(25) Pan, C. J.; Lee, Y. J.; Ammundsen, B.; Grey, C. P. *Chem. Mater.* **2002**, *14*(5), 2289–2299.

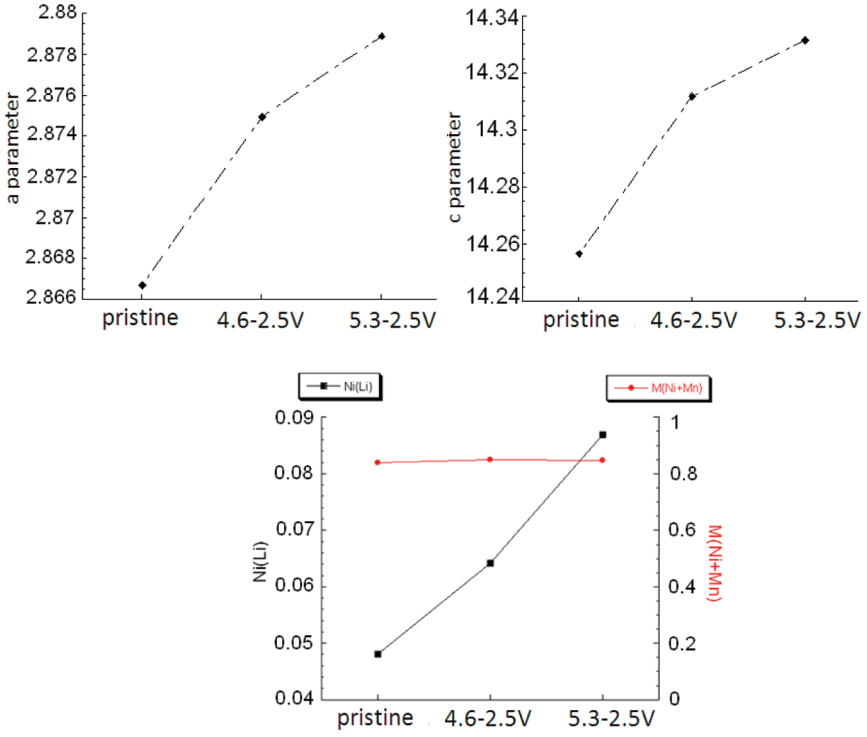

Figure 10. Results from the structural refinements for the pristine and two discharged samples. (a, b) Plots of the *a* and *c* cell parameters for the three samples. (c) Plot of the metal content in the Li layers (black line) and total transition metal content in the transition metal layers (red line).

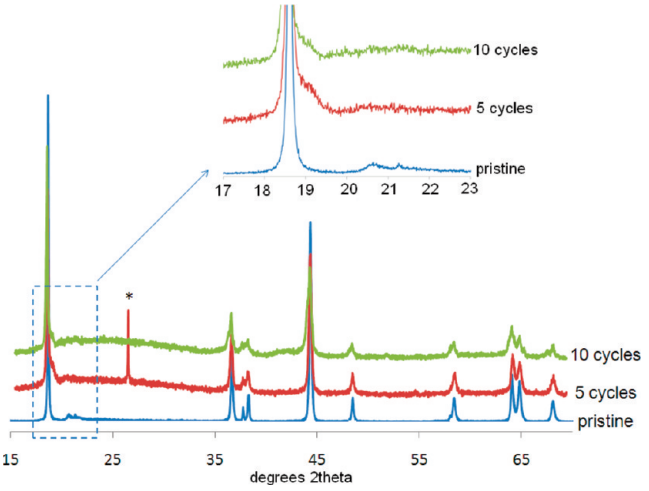

Figure 11. Comparison of the XRD pattern of the multiply cycled, fully discharged samples cycled with cutoff voltage windows of 4.6−2.5 V and the pristine material. The inset is an enlargement of the superstructure peaks region. The sharp peak marked with an asterisk observed in the 5 cycles sample is from graphite.

and second cation coordination shells of Li. The broad peak at 737 ppm is similar to that seen for the Li ions in the lithium layers of Li_2MnO_3,[26] while the resonance at 1511 ppm is at the shift position for Li in the predominantly manganese layers of Li_2MnO_3, and is hence assigned to Li^+ in the transition metal layers, surrounded by 6 Mn^{4+} ions ($Li(OMn)_6$). The resonance at 1341 ppm is assigned to Li^+ surrounded by 5 Mn^{4+} and 1 Ni^{2+} ion.

(26) Breger, J.; Jiang, M.; Dupre, N.; Meng, Y. S.; Shao-Horn, Y.; Ceder, G.; Grey, C. P. *J. Solid State Chem.* **2005**, *178*(9), 2575–2585.

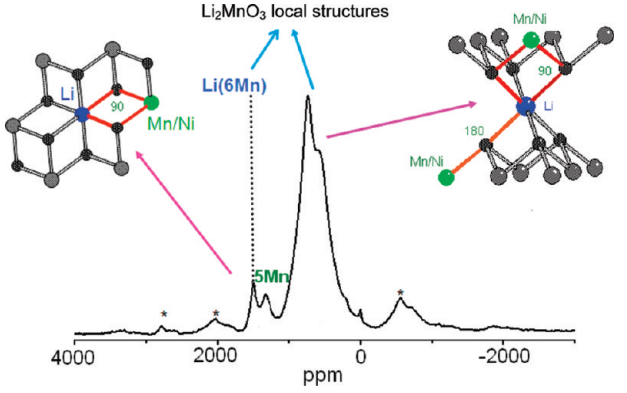

Figure 12. ^{6}Li MAS NMR spectrum of pristine $Li[Li_{1/9}Ni_{1/3}Mn_{5/9}]O_2$ acquired at a spinning speed 38 kHz. The sidebands due to magic angle spinning are marked with asterisks. The two main classes of Li local environments expected for Ni^{2+}-substitution in a Li_2MnO_3-type local environment are shown.

Figure 13 shows the ^{6}Li NMR spectra of $Li[Li_{1/9}Ni_{1/3}Mn_{5/9}]O_2$ as a function of the state of charge. The spectra have been normalized with the total number of scans and the weight of active material packed in the rotors, so that the intensity of each resonance can be directly related to the number of Li ions in each sample, assuming that the spin−lattice relaxation times T_2 values are similar for the different sites. (We note that since a very fast MAS was used (38 kHz), the time between the end of the excitation pulse and the detection (i.e., the sum of the evolution and refocusing times) used in the spin−echo experiment was extremely short (53 μs). Under these conditions, the corrections that need to be applied to the relative intensities to take into account any differences due to variations in the T_2 values are small for the hyperfine-shifted resonances studied in this system, which

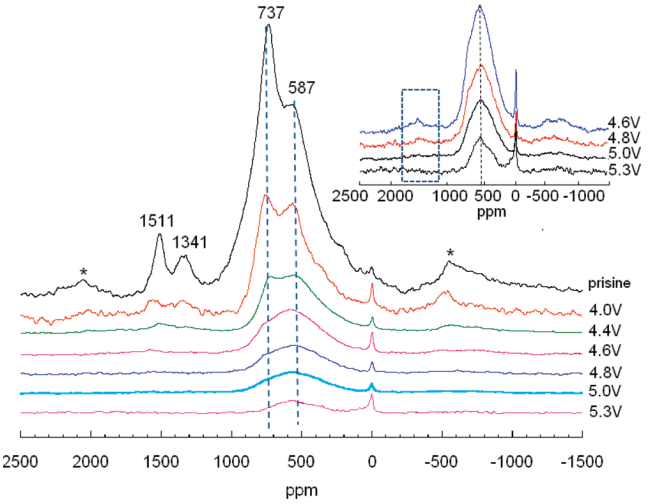

Figure 13. ^{6}Li MAS NMR spectra of the charged samples acquired at a 38 kHz spinning speed. Sidebands are marked with asterisks. The inset shows an enlargement of the spectra of the high voltage samples; the dashed blue box in this inset shows the location of the resonances due to Li in the predominantly transition metal layers.

have T_2 values several orders of magnitude larger than 53 μs). When the compound is charged to 4.4 V, the intensity of the peaks ascribed both to Li in the lithium layers and Li in the transition metal layers decrease, as previously observed,[24] indicating that lithium is removed from both layers. At 4.6 V, the 737 ppm peak due to Li environments in the Li layers resembling those in Li_2MnO_3 has decreased noticeably in intensity and appears to be buried under a broader peak centered at 500−600 ppm. This latter peak likely contains Li environments in the Li layer where the Li is nearby Ni^{4+} (diamagnetic) ions and/or Li in the tetrahedral sites, adjacent to the Li vacancies in the transition metal layers. In contrast, the Li ions in the transition metal layers are still not completely removed at this voltage. The results should be contrasted with the Li NMR spectra of $Li[Co_{1/3}Mn_{1/3}Ni_{1/3}]O_2$ and M-doped $LiCoO_2$ and $LiNiO_2$, where Li removal is accompanied by the coalescence and/or gradual shifting of the Li resonances, particularly at higher states of charge. This is ascribed to rapid Li and/or electronic mobility, which does not appear to be occurring here, at least on the NMR time scale.[27,28] From 4.6 to 5.3 V, the intensity of the peaks around 600 ppm gradually decreases, consistent with the removal of lithium from the structure, and thus, with the compound still being electrochemically active at these voltages. The continuous Li removal from the structure is consistent with the results observed for $Li_{1.12}[Ni_{0.425}Mn_{0.425}Co_{0.15}]O_2$, where the removal of Li during this plateau is confirmed by chemical Li titration.[29] No peaks around 1500 ppm are observed at 5.3 V, and only one broad symmetric peak remains at around 600 ppm, indicating that all the Li ions have been removed from the transition metal layers, but also that there are still some Li ions left in the lithium layers. No extra peaks are observed in the charged materials except for one at 0 ppm, which arises from the Li ions in diamagnetic environments in the electrolyte salt ($LiPF_6$) or in the passivation layer on the surface of the electrode.[30] This peak becomes broader and slightly more intense in the 5.3 V sample, which is consistent with the electrolyte decomposition, a thicker passivation layer being produced in this process.

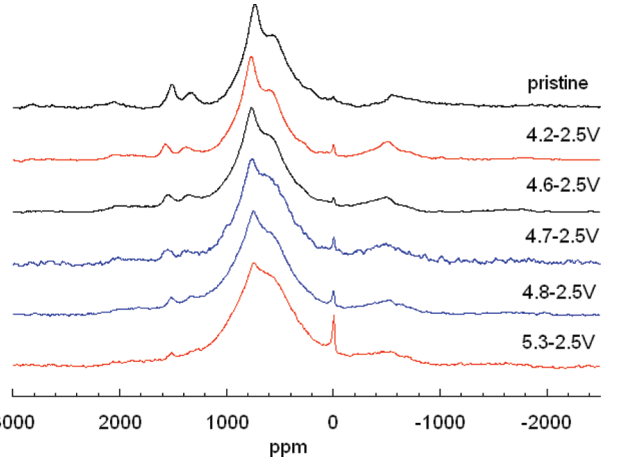

Figure 14. ^{6}Li MAS NMR spectra of discharged samples.

A similar study was also performed on a series of samples prepared after one charge−discharge cycle, and the NMR spectra of discharged samples are displayed in Figure 14. The low natural abundance of ^{6}Li (7.43%) and the fact that the electrolyte and Li metal used in the batteries is not enriched in ^{6}Li means that the Li content in these samples can no longer be readily quantified on the basis of the intensity of the ^{6}Li spectra, which represents the ^{6}Li content in the sample, and not necessarily the total Li content. Thus, the spectra for all the discharged samples shown in Figure 14 and 15 are not normalized. The two sets of resonances ascribed above to Li in the Li, and in the transition metal layers, are still present in all the spectra. As before, the peaks at 0 ppm correspond to the presence of diamagnetic electrolyte/SEI environments. Two trends can be observed in the spectra as a function of maximum voltage on charge. First, the intensity of the peaks around 1500 ppm gradually decreases as the charge cutoff voltage is increased, and these peaks are almost absent in the 5.3−2.5 V sample, indicating that only very few Li ions can be reintercalated into the transition metal layers on discharge after charging at high voltages. Second, the broad peak centered at 750 ppm becomes much more symmetric and featureless, in comparison to the same resonance in the pristine sample, for the sample cycled over a larger voltage window. This is the evidence of cation rearrangement in the transition metal layers at high voltages. Taken together, this appears to suggest that either some of the vacancies left behind in the transition metal layers after the Li ions are removed from the transition metal layers are occupied by the other transition metal ions which can migrate from the adjacent

(27) Chazel, C.; Menetrier, M.; Croguennec, L.; Delmas, C. *Inorg. Chem.* **2006**, *45*(3), 1184–1191.
(28) Levasseur, S.; Menetrier, M.; Delmas, C. *J. Electrochem. Soc.* **2002**, *149*(12), A1533–A1540.
(29) Tran, N.; Croguennec, L.; Menetrier, M.; Weill, F.; Biensan, P.; Jordy, C.; Delmas, C. *Chem. Mater.* **2008**, *20*(15), 4815–4825.
(30) Meyer, B. M.; Leifer, N.; Sakamoto, S.; Greenbaum, S. G.; Grey, C. P. *Electrochem. Solid-State Lett.* **2005**, *8*(3), A145–A148.

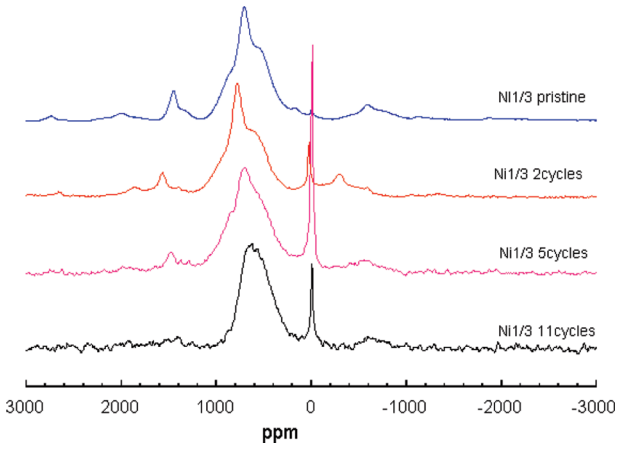

Figure 15. ^{6}Li MAS NMR spectra of the multiple cycled discharged samples with a cutoff voltage window of 4.6−2.5 V.

sites or that significant rearrangement of Ni and Mn ions within the layers occurs. As a result, the honeycomb ordering is lost and the available sites for lithium reinsertion are either no longer present or not as energetically favorable, which is one possible reason why no lithium goes back to the transition metal layers on reduction to 2 V. The ^{6}Li NMR results provide compelling evidence of a continued structural change of the material during the high voltage plateau.

The ^{6}Li NMR spectra of multiple cycled samples are compared in Figure 15. In the pristine compound, the peak at around 1340 ppm has a lower intensity compared to the intensity of the similar resonance shown in Figure 12 and 13, indicating that more ordering is present in this sample because of the slightly different synthesis conditions. All the cycled samples were charged to 4.6 V and discharged to 2.5 V. The trend is similar to that observed in Figure 14. The peaks at around 1500 ppm become less pronounced as a function of the number of cycles, and they totally disappear in the discharged sample after 11 cycles. This suggests that the lithium can not be intercalated back to the transition metal layers after multiple cycles. The peak corresponding to the Li in Li layers is much more symmetric compared to that in the pristine compound, indicating a cation rearrangement in the transition metal layers as discussed previously. The spectrum of the 11 cycles sample is actually very similar to the sample cycled between 5.3 and 2.5 V. This is also consistent with the XRD data (Figure 11). The final structure of the multiple cycled sample with lower cycling voltage window (4.6−2.5 V) is similar to the sample cycled between the high voltage window (5.3−2.5 V), Li largely being located in the lithium layers, the honeycomb ordering (and Li substitution) having disappeared in the transition metal layers.

3.4. X-ray Absorption Spectroscopy (XAS). To study the change in the oxidation state of the transition metal ions during the electrochemical processes that take place in a battery, we performed XAS experiments on a series of cycled samples. Normalized Ni and Mn K-edge X-ray absorption near edge structure (XANES) spectra of cycled samples are displayed in Figure 16. Previous studies[4,24,31] have shown that Ni^{2+} and Mn^{4+} coexist in $Li[Li_{1/9}Ni_{1/3}Mn_{5/9}]O_2$. At 4.6 V, all the Ni^{2+} ions were found to be oxidized to Ni^{4+}, whereas the Mn^{4+} ions remain in the same oxidation state. However, the possible changes at higher voltages, such as 5.3 V, have not been evaluated before. Figure 16a shows the Ni K-edge spectra of the charged samples. The absorption edge gradually shifts to higher energy as the compound is charged to 4.4 V, which is consistent with the oxidation of Ni^{2+}. A small shift takes place when the voltage is increased to 4.6 V, but, contrary to what would be expected, when the voltage rises above 4.6 V, the position of the main edge, which corresponds to the transition between 1s → 4p involving a "shake-down" process caused by a ligand-to metal charge transfer (LMCT),[31−33] actually shifts back to lower energies, but the higher component of the edge corresponding to the dipole-allowed 1s → 4p transition without a shake-down process shifts in the opposite direction, and the whole shape of the spectra is different from that of the pristine compound, suggesting a significant local environment change of Ni ions at these voltages.

The Ni K-edge spectra of the three samples which were charged to different voltages, and discharged to 2.5 V, are compared with that of $Li[Li_{1/9}Ni_{1/3}Mn_{5/9}]O_2$ in Figure 16b. Both the shape and the edge position of these samples are very similar to that of the pristine compound, even for the sample which has been charged to 5.3 V. Hence, all the Ni ions seem to be reduced to Ni^{2+} at the end of discharge. Figure 16c shows the Mn K-edge spectra of the same samples. The spectrum of the 4.6−2.5 V sample is very similar to that of the starting phase. In contrast, the spectra of both 4.8−2.5 V and 5.3−2.5 V samples are different, which is an indication of a change in the Mn local environment as the compound is charged to high voltages because the shape of the Mn edge is very sensitive to the local geometry of the Mn atoms.[4,34] The change of the local environment is ascribed to the rearrangement of the transition metal ions. Despite this shape change, the spectra do not show a solid shift, which indicates that the Mn ions are in the same oxidation state as in $Li[Li_{1/9}Ni_{1/3}Mn_{5/9}]O_2$, and no reduction occurs upon the intercalation of Li.

3.5. TEM. TEM experiments were performed to study the morphology changes upon electrochemical cycling of $Li[Li_{1/9}Ni_{1/3}Mn_{5/9}]O_2$. Figure 17a shows the TEM micrograph of a sample charged up to 5.3 V. A thick passivation layer of about 10−20 nm is observed on the surface of the electrode, which is ascribed to surface side reactions between the electrode and the electrolyte. In addition, obvious particle cracking was found in certain regions of some crystals (for instance, the expanded view of the

(31) Yoon, W. S.; Grey, C. P.; Balasubramanian, M.; Yang, X. Q.; McBreen, J. *Chem. Mater.* **2003**, *15*(16), 3161–3169.
(32) Kim, M. G.; Yo, C. H. *J. Phys. Chem. B* **1999**, *103*(31), 6457–6465.
(33) Pickering, I. J.; George, G. N. *Inorg. Chem.* **1995**, *34*(12), 3142–3152.
(34) Balasubramanian, M.; McBreen, J.; Davidson, I. J.; Whitfield, P. S.; Kargina, I. *J. Electrochem. Soc.* **2002**, *149*(2), A176–A184.

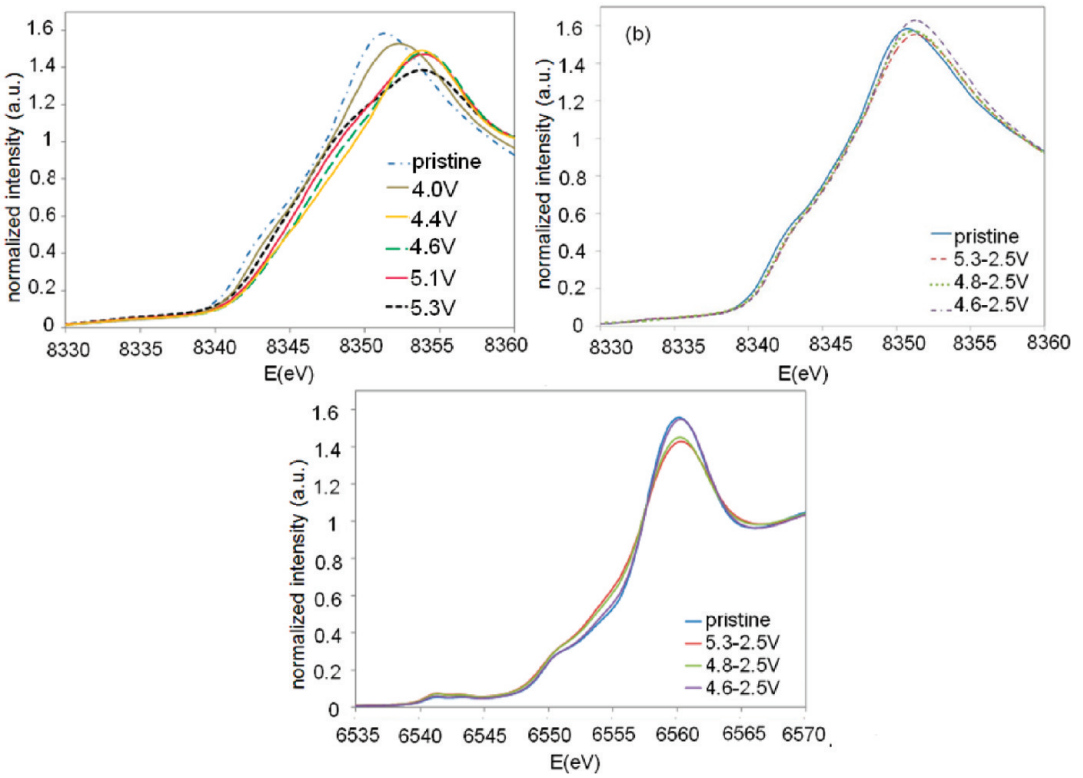

Figure 16. Normalized X-ray absorption near edge structure (XANES) Ni and Mn K-edge spectra for the pristine and cycled $Li[Li_{1/9}Ni_{1/3}Mn_{5/9}]O_2$ samples. Ni K-edge on (a) charge and (b) discharge and (c) the Mn K-edge of the discharged samples.

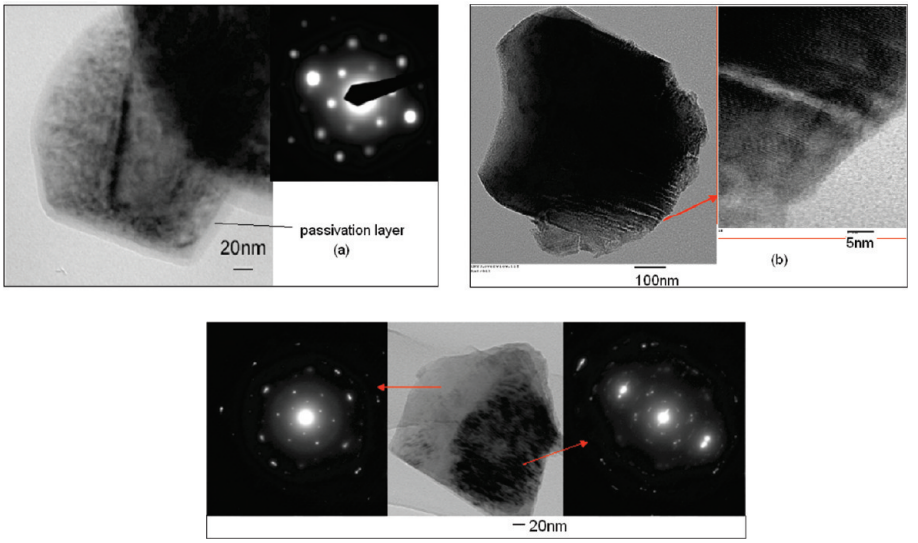

Figure 17. High-resolution TEM pictures of cycled $Li[Li_{1/9}Ni_{1/3}Mn_{5/9}]O_2$: (a) charged sample stopped at 5.3 V, (b, c) two particles from an electrode charged to 5.3 V then discharged back to 2.5 V.

region marked with an arrow in Figure 17b) of a sample charged to 5.3 and discharged to 2.5 V. A similar phenomenon was observed by Lei et al.[35] in their HREM study, which was also ascribed to oxygen loss. Other crystals from the same sample even show distinct diffraction domains, as revealed by the electron diffraction patterns of two different parts of the same particle in Figure 17c. Different crystallinity is clearly observed; although one side of the particle is still single crystalline (i.e., results in well-resolved diffraction spots in the pattern), the diffraction pattern of the other is composed of less well-defined spots with considerable streaking. This streaking is most probably associated with a formation of nanosized domains (shown in Figure 17c), resulting in a change in the microstructure.

3.6. Analysis of the Evolved Gases. Two separate batteries were arrested at the ends of the electrochemical plateaus at approximately 4.6 V and 5.3 V. An analysis of the evolved gases from these two batteries showed a mixture of Ar, CO_2, and CO, Ar representing the major component. CO_2 was found to be the second major

(35) Lei, C. H.; Bareno, J.; Wen, J. G.; Petrov, I.; Kang, S. H.; Abraham, D. P. *J. Power Sources* **2008**, *178*(1), 422–433.

component in the mixture after Ar. No significant O_2 components were observed. The absence of any leaks in the battery were confirmed by monitoring the N_2:O_2 ratio, the absence of N_2 confirming that no leak was present. The experiment was repeated for several batteries and similar results were obtained. The Li anode was also inspected for proof for reaction with O_2. No discernible evidence of Li_2O was observed for batteries arrested at 4.4, 4.6, and 5.3 V. The results suggest that, in comparison to previous results based on in situ gas analysis, either when the evolved O_2 is allowed to remain in the cell it results in electrolyte decomposition (but surprisingly, little attack of the Li metal), or that part of the oxygen loss mechanism involves the direct oxidation of the electrolyte. This is discussed later on in the paper.

4. Discussion

The results of both the GITT and the PITT experiments confirm the existence of a plateau at around 4.5 V upon the first charge of a battery containing $Li[Li_{1/9}Ni_{1/3}Mn_{5/9}]O_2$ as a positive electrode. The NMR results indicate that although some of the capacity observed in this region is associated with electrolyte decomposition, it must also be accompanied by removal of Li^+. Previous studies have proposed that the plateau at 4.5 V is due to the oxygen loss mechanism,[8] and that the removal of Li is accompanied by the loss of oxygen, resulting in an irreversible net loss of Li_2O from the structure. Mantia et al. have demonstrated direct evidence of oxygen evolution from the Li-excess material $Li_{1+x}(Ni_{1/3}Mn_{1/3}Co_{1/3})_{1-x}O_2$ at high potentials by in situ differential electrochemical mass spectrometry (DEMS).[36] Oxygen gas was only observed in the Li-excess material during the first cycle, but not in the following cycles, and in the stoichiometric ($x = 0$) material. CO_2 was also detected in both systems (Li-excess and stoichiometric) during the first cycle. However, it was absent in the Li-excess material in the second cycle, and yet was still observable in the stoichiometric sample. The absence of CO_2 evolution in the Li-excess system in the second cycle was ascribed to the formation of a surface film composed of an electrolyte oxidation product during the first cycle. Our TEM micrographs (for example, see Figure 17a) provide direct evidence of this passivation layer formation on the surface. The NMR spectra of the materials charged to high voltages also contain strong signals at close to 0 ppm, the signals primarily arising from diamagnetic components in the SEI.

We were unable to detect any O_2 in our ex situ studies of the gas evolution on charging to 4.6 and 5.3 V. On the basis of these results, we propose that at least some of the oxygen loss, which must accompany the Li^+ removal, is associated with the direct oxidation of DMC (Dimethyl Carbonate) and/or ethyl carbonate (EC) in the electrolyte by the highly oxidized electrode material. In this mechanism, the EC or DMC is oxidized to an aldehyde (or ketone) formally by the oxide ions in the electrode material, with CO_2 and H_2O being generated as by-product. The resulting aldehyde can further react with other O^{2-} ions to yield carboxylic acids, as shown in the scheme drawn below (for DMC as example)

$$CH_3{-}O{-}C(O){-}O{-}CH_3 + 4Ni^{4+} + 2O^{2-} \rightarrow 2CH_2O + CO_2 + H_2O + 4Ni^{3+} \quad (1)$$

$$CH_2O + 2Ni^{4+} + O^{2-} \rightarrow HCO_2H + 2Ni^{3+} \quad (2)$$

$$Ni^{3+} \rightarrow Ni^{4+} + e^- \quad (3)$$

The different steps presumably occur simultaneously, the removal of Li^+ (which will accompany reaction 3) driving the processes. It is important to note that the first two reactions are not associated with current flow in the cell. The Ni^{4+}/Ni^{3+} may be thought of as a catalyst for the electrolyte decomposition and O^{2-} loss mechanism, the Ni^{4+} being regenerated electrochemically. This process results in a capacity that is higher than the 200 mA h g^{-1} capacity expected solely from the oxidation of the initial Ni^{2+} ions. The in situ results of Mantia et al.[36] indicate that direct O^{2-} oxidation (without the involvement of the electrolyte) does occur to some degree. Thus a second possible explanation for the lack of O_2 in our systems is that any O_2 generated, from the direct oxidation of O^{2-} to O_2 (without the involvement of the electrolyte), can react with the electrolyte to form CO_2. This mechanism may become dominate in our closed system, because the O_2 cannot escape from the sealed battery. Because the electrolytes are stable in air, this mechanism must again be accompanied (and catalyzed) by a second reaction involving the electrode materials. The particle cracking seen by TEM suggests that at least some of the oxygen loss occurs from within the particles. This mechanism presumably does not result directly in electrolyte decomposition. On the basis of our preliminary studies, we note that particle cracking is mostly observed in large particles such as the one observed in Figure 16b, indicating that importance of the two mechanisms may vary as a function of particle size.

Our ^{6}Li NMR results can now be used to evaluate which sites are vacated by the removal of Li^+ ions and the sequence of extraction during charge process. First, from an OCV of 3.5 V to 4.6 V, 2/3 of the Li^+ ions are removed through via charge compensation of the oxidation of Ni^{2+} to Ni^{4+}. These ions are extracted from both lithium layers and transition metal layers, and most of the lithium in transition metal layers are removed at this voltage, as seen by the almost complete disappearance of the 1500 ppm peak in the ^{6}Li NMR spectra of the 4.6 V sample. Our samples appear to show some heterogeneity, as two phases are seen at this point by XRD. It is not clear whether the minor phase is a spinel or a layered phase, but spinel domains are frequently observed in the electron diffraction results for some of the particles in this voltage

(36) La Mantia, F.; Rosciano, F.; Tran, N.; Novak, P. *J. Appl. Electrochem.* **2008**, *38*, 893–896.

range. The loss of 1/9 Li ions (per formula unit) from the transition metal layers results in vacancies in these layers, which then allow 2/9 Li tetrahedral sites (per formula unit) in the lithium layers, on either side of these vacancies to be occupied, as discussed in earlier papers for the $Li(Ni_{0.5}Mn_{0.5})O_2$ material.[20,37,38] Although the predicted NMR shifts for Li in tetrahedral sites and octahedral sites are very close in this system, the NMR spectra are consistent with this proposal. The ideal formula of the material at this point is $Li_{2/9oct}Li_{2/9tet}[\square_{1/9}Ni_{1/3}Mn_{5/9}]O_2$, and all of the Ni ions are present as Ni^{4+}. Our neutron diffraction results of the $Li(Ni_{0.5}Mn_{0.5})O_2$ sample, where vacancies are also formed in the transition metal layers, showed that the concentration of tetrahedral sites was lower than predicted based on the concentration of vacancies (and the octahedral sites were correspondingly higher), presumably because of repulsions between Li ions in the tetrahedral sites, when two such occupied sites are nearby.

On the basis of the GITT results, a plateau at approximately 4.5 V is seen, and after the theoretical capacity has been obtained, another 63 mA h g^{-1} of capacity is observed (i.e., until 4.8 V is reached in the experiments performed galvanostatically). This is ascribed to the loss of further Li, accompanied by the loss of oxygen. 63 mA h g^{-1} corresponds to 0.2 Li, and an analysis of the intensities of the NMR spectra of the 4.6 and 4.8 V samples indicates that the Li removal corresponds to roughly 2/3 of this capacity, indicating that although electrolyte decomposition occurs, it is not the dominant process. We propose that Li ions from the octahedral sites are lost at this point

$$Li_{4/9}[\square_{1/9}Ni_{1/3}Mn_{5/9}]O_2 \rightarrow Li_{0.24}[\square_{1/9}Ni_{1/3}Mn_{5/9}]O_{1.9} + 0.05O_2 + 0.2\ Li^+ + 0.2e^- \quad (4)$$

A dramatic increase in the potential is now seen on charging, but the OCV is similar. We ascribe this noticeable increase to either the additional potential required to remove Li from the tetrahedral sites, as proposed previously for $Li(Ni_{0.5}Mn_{0.5})O_2$,[20,37,38] and/or an additional overpotential caused by the formation of by now an increasingly thick passivating film on the surface. However, if the latter explanation were valid, we might expect the voltage to increase steadily during this process >5 V because the electrolyte decomposition is now significant in this voltage window, which it does not. For the former process to correct, the Li loss must be accompanied by a further structural rearrangement, so that the OCV drops back down to 4.6 V. Referring back to the $Li(Ni_{0.5}Mn_{0.5})O_2$ system, here we ascribed the >5.0 V high voltage process to a combination of Li loss from the tetrahedral sites and the migration of Ni (in this case from the Li layer to the transition metal layer). It is again possible that a similar process is occurring here, the migration now involving the filling in of the vacancies in the Li layers by cations predominantly in the transition metal layers. At the end of the process, almost all of the Li is removed from the material.

If Ni and Mn migration occurs to fill in the vacancies in the transition metal layers, as shown by Armstrong et al. for the their lower Ni content material $Li[Li_{1/5}Ni_{1/5}Mn_{3/5}]O_2$,[8] then the formula for the 4.8 V sample should be rewritten as $Li_{0.26}[\square_{0.06}Ni_{0.35}Mn_{0.59}]O_2$. This formula requires that some Li move from the tetrahedral sites back onto octahedral sites as the vacancies in the transition metal layers are filled. These, according to our hypothesis, should also be removed at a potential of approximately 4.5 V, extending the length of this plateau. On discharge an increased concentration of Ni is seen in the Li layers, and it is not clear whether this migration occurs at high voltages or on the subsequent discharge. It seems more plausible, however, that at least some of the Ni or Mn ions that migrate at high voltages to fill the vacant sites in the transition metal layers also occupy some sites in the Li layers, most likely occupying sites above and below vacancies in the transition metal layers, forming small spinel-like structural motifs in the solid. Another additional complexity that we have not addressed is the mechanism by which the Ni and Mn ions move in this system, and the consequences of their differences in mobility, on the phases that are formed. Differences in mobility between the two components may lead to nonuniform Ni/Mn distributions and/or metastable phases. Thus, a third possible explanation for the higher voltage processes is that it is either linked with the migration of a different transition metal cation, or a transition metal cation from one site to another. We note that the particle cracking sometimes observed means that O^{2-} ions can be lost from not just the original surface of the particle, reducing the diffusion lengths over which the cations must migrate to fill the cation vacancies.

On discharge, all the Ni^{4+} is reduced back to Ni^{2+}, the oxidation of the Mn^{4+} remaining unchanged, resulting in a material with nominal stoichiometry $Li_{2/3}[Ni_{3/8}Mn_{5/8}]O_2$, assuming the ideal layered structure model of Armstrong et al.[8] The NMR of this sample confirms that considerable rearrangements of the Ni and Mn have occurred in the transition metal layers, the signal broadening considerably, as compared to the original sample. The Mn and Ni XAS data also suggest that the local environments change noticeably during the high voltage processes. The question remains – why can the Mn^{4+} not be reduced further in this material, if there are still vacancies in the Li layers, which must be present if an ideal layered structure is formed? The simplest explanation is that the presence of metal ions in the Li layer block possible sites for Li in both the Li and metal layers (in a material containing vacancies in these layers). Li may not also return to the transition metal layers even if there are vacancies, because of the rearrangement of the cations in the transition metal layers. Vacancies in the metal layers surrounded predominantly by Ni^{2+} ions will

(37) Grey, C. P.; Yoon, W. S.; Reed, J.; Ceder, G. *Electrochem. Solid-State Lett*. **2004**, *7*(9), A290–A293.
(38) Van der Ven, A.; Ceder, G. *Electrochem. Commun*. **2004**, *6*(10), 1045–1050.

be less favorable for Li^+. Interestingly, a redox process that is likely due to Mn^{4+} reduction, at close to 3 V, is sometimes seen for samples that were charged to only 4.6 V (see Figure 2a), but this disappears in the samples charged to higher voltages. This also disappears for samples cycled over multiple cycles to 4.6 V, the NMR results confirming that local structures in these samples eventually resemble the material that has undergone only one charge−discharge cycle to 5.3 V. Thus, it appears that a metastable (or intermediate) phase that is formed after one charge to 4.6 V, but that after multiple cycles it starts to resemble the end structure that is created in one cycle, following cycling to higher voltages. Finally, it is worth noting that the stable structure that is created by either high-voltage or by extended cycling involves significant cation rearrangements and is produced as a result of a structural rearrangement that occurs at low lithium contents, in a material involving predominantly M^{4+} ions. Thus, simple pretreatments of the material, e.g., by acid leaching,[39] are unlikely to result in the same structural changes. Different pretreatment strategies are required.

5. Conclusions

The electrochemical behavior of layered $Li[Li_{1/9}Ni_{1/3}Mn_{5/9}]O_2$ as a positive electrode in lithium batteries has been investigated in this study. Three distinct processes are seen on charging to 5.3 V, the GITT and PITT experiments confirming that the first processs from 3.6 up to approximately 4.4 V involves a solid solution, whereas the two apparent plateaus at approximately 4.5 and 5.0 V are associated with a two phase reaction, both with an OCV of close to 4.5 V. Both higher capacity and better capacity retention are obtained after the material has been charged to this higher voltage.

The ^{6}Li MAS NMR spectra show that the Li ions are removed from both the lithium and the transition metal layers upon charge, even at voltages above 4.6 V, which is clear evidence that the capacity obtained at these high voltages is not solely due to electrolyte decomposition. The high-resolution XRD patterns show that the honeycomb ordering in the transition metal layers is lost when charging at 5.3 V, which is likely to be associated with a migration of transition metal ions into the vacancies left by the extracted lithium ions. A second phase is also seen above 4.4 V, possibly indicating some heterogeneity in our samples. The ^{6}Li MAS NMR spectra of these samples also show that very few Li ions can be intercalated back into the transition metal layers after being charged at very high voltages, in agreement with the absence of honeycomb type superstructure peaks in the XRD patterns of the discharged samples. The change of the ^{6}Li NMR line shape is indicative of significant rearrangement of transition metal ions in these layers, while the Rietveld refinements of these discharged samples show an increase in the Ni content in the Li layers, which is ascribed to the cation migration that occurs at high voltages.

The Ni K-edge XANES spectra show that the Ni is oxidized during the solid solution. The evolution of the Ni edge is more complicated during the high voltage plateaus, and is ascribed to a change of local structure that occurs in this regime. The Mn K-edge XANES spectra of the different cycled samples suggests a change in the local environment of the Mn^{4+} ions, but no obvious reduction is observed. High-resolution TEM pictures show the formation of a passivation layer on the surface of the electrode particles at high voltages. In addition, cracking and nanosize domains were observed in some crystals after charging to 5.3 V, the former being ascribed to oxygen loss. However, no oxygen was observed in our ex situ m.s. analysis of the gases evolved from the battery, the oxygen presumably reacting with the electrolyte.

Acknowledgment. The work was supported by the Assistant Secretary for Energy Efficiency and Renewable Energy, Office of FreedomCAR and Vehicle Technologies of the U.S. Department of Energy under Contract DE-AC03-76SF00098, via Subcontract 6517749 with the Lawrence Berkeley National Laboratory. Y.S.M. acknowledges the new faculty startup fund by University of Florida for financial support. Use of the Advanced Photon Source (APS) was supported by the U.S. Department of Energy, Office of Science, Office of Basic Energy Sciences, under Contract W-31-109-Eng-38. We thank Dr. Peter Lee for collecting XRD data at APS, and Dr. Jordi Cabana Jiménez, Dr. Denis Yu, Prof. Gerbrand Ceder, and Prof. Yang Shao Horn for helpful discussions.

(39) Kang, S. H.; Johnson, C. S.; Vaughey, J. T.; Amine, K.; Thackeray, M. M. *J. Electrochem. Soc.* **2006**, *153*(6), A1186–A1192.